

EgoEvGesture: Gesture Recognition Based on Egocentric Event Camera

LUMING WANG,^{1,†} HAO SHI,^{1,†} XIAOTING YIN,¹ KAILUN YANG,² AND KAIWEI WANG^{1,*}

¹*State Key Laboratory of Extreme Photonics and Instrumentation, Zhejiang University, Hangzhou 310027, China*

²*National Engineering Research Center of Robot Visual Perception and Control Technology, Hunan University, Changsha 410082, China*

[†]*Equal contribution*

^{*}wangkaiwei@zju.edu.cn

Abstract: Egocentric gesture recognition is a pivotal technology for enhancing natural human-computer interaction, yet traditional RGB-based solutions suffer from motion blur and illumination variations in dynamic scenarios. While event cameras show distinct advantages in handling high dynamic range with ultra-low power consumption, existing RGB-based architectures face inherent limitations in processing asynchronous event streams due to their synchronous frame-based nature. Moreover, from an egocentric perspective, event cameras record data that include events generated by both head movements and hand gestures, thereby increasing the complexity of gesture recognition. To address this, we propose a novel network architecture specifically designed for event data processing, incorporating (1) a lightweight CNN with asymmetric depthwise convolutions to reduce parameters while preserving spatiotemporal features, (2) a plug-and-play state-space model as context block that decouples head movement noise from gesture dynamics, and (3) a parameter-free Bins-Temporal Shift Module (BSTM) that shifts features along bins and temporal dimensions to fuse sparse events efficiently. We further build the EgoEvGesture dataset, the first large-scale dataset for egocentric gesture recognition using event cameras. Experimental results demonstrate that our method achieves 62.7% accuracy in heterogeneous testing with only 7M parameters, 3.1% higher than state-of-the-art approaches. Notable misclassifications in freestyle motions stem from high inter-personal variability and unseen test patterns differing from training data. Moreover, our approach achieved a remarkable accuracy of 96.97% on DVS128 Gesture [1], demonstrating strong cross-dataset generalization capability. The dataset and models are made publicly available at https://github.com/3190105222/EgoEv_Gesture.

1. Introduction

Gesture recognition is a pivotal technology in fields such as computer vision [2], human-computer interaction [3], virtual reality [4], and robotics [5]. Egocentric gesture recognition, which captures actions from a first-person perspective, stands out for its natural and intuitive interaction modality, making it highly suitable for seamless integration into daily life. This has significant implications for Extended Reality (XR) [6], smart wearable devices [7], and human-computer interaction in various domains [8]. Unlike third-person settings, egocentric perspectives place sensors closer to the action, inherently incorporating natural attentional cues derived from the human line of sight.

However, existing approaches that rely on traditional frame-based cameras are ill-suited for dynamic environments typical of egocentric perspectives. Traditional cameras, which capture images at fixed frame rates, often struggle with motion blur and sudden changes in lighting. These limitations are particularly pronounced in low-light conditions, where the reduced amount of available light exacerbates motion blur and makes it challenging to capture clear and usable images. Additionally, the continuous frame capture nature of traditional cameras results in high power consumption and memory requirements, further limiting their practicality for wearable devices and real-time applications [9, 10].

Event cameras, on the other hand, offer a promising alternative. These cameras asynchronously measure intensity changes at the pixel level, generating neuromorphic events with very high temporal resolution (on the order of microseconds), virtually no motion blur, and high dynamic range (HDR, 120 dB). They also consume significantly less power and memory compared to traditional frame-based cameras, thus making them highly suitable for real-world applications such as egocentric action recognition on wearable devices [10–12]. Despite these advantages, egocentric gesture recognition presents a significantly larger challenge for event cameras compared to conventional frame-based cameras: 1) In third-person settings, events are primarily generated by the motion of the observed subject. In contrast, in egocentric perspectives, events are generated by both the motion of the camera (due to head movements) and the motion of the hands performing gestures. This dual source of motion complicates the interpretation of event data, as it becomes difficult to disentangle the camera’s ego-motion from the actual gesture movements. Consequently, the gap between third-person and egocentric gesture recognition is more pronounced for event cameras than for traditional cameras, making the task significantly more challenging. 2) In addition, the development of egocentric gesture recognition using event cameras has been hindered by the lack of large-scale, well-annotated datasets as well.

To address these challenges, we first propose a novel approach with three progressive processing stages, as illustrated in Figure 6. First, we convert raw events into Locally Normalized Event Surfaces (LNES) [13] that focus on the most recent temporal signature, suppressing historical ego-motion artifacts while maintaining real-time performance. Second, we employ Blaze [14] & Vision Mamba [15] (VMamba) blocks to extract spatiotemporal features. The Blaze encoder-decoder, adapted from [14] with proven efficiency in human-centric perception [16], processes each temporal bin efficiently. The VMamba block [15] addresses sparse event processing and long-term temporal modeling through discrete state space

equations. Finally, we propose the Bins-Temporal Shift Module (BTSM), a zero-parameter mechanism that shifts features bidirectionally along two orthogonal axes: 1) Bins axis (fine temporal resolution: 33 ms/bin) for inter-bin context fusion, 2) Raw temporal axis (coarse resolution: 200 ms) for intra-bin motion alignment. This dual-scale shifting resolves temporal fragmentation while maintaining motion invariance. Due to the lack of event datasets in the egocentric setting, we developed EgoEvGesture, the first large-scale dataset for egocentric gesture recognition using event cameras. Captured under both normal and low-light conditions, it includes data from 10 subjects performing a variety of gestures, offering rich temporal and spatial information for training and evaluating models in real-world scenarios. Our proposed method achieves a classification accuracy of 62.7% on this dataset, with only 7M parameters, outperforming existing (closely related) approaches by 3.0%. To verify the effectiveness of our approach, we evaluated it on the DVS128 Gesture dataset [1], achieving a competitive accuracy of 96.97%. This result highlights the robustness of our architecture in handling sparse and temporally challenging event-based data. The significance of each proposed module is evaluated and confirmed in an ablation study.

In summary, this paper defines a new problem, i.e. gesture recognition based on egocentric event camera, and makes the following technical contributions:

- **Construction of the first large-scale, real-world egocentric event-based gesture estimation dataset, EgoEvGesture:** Contains event sequences from 10 subjects performing 38 actions under both normal and low light conditions, with accurate action annotations.
- **Bins-Temporal Shift Module (BTSM):** A zero-parameter mechanism enabling dual-axis feature shifting across bins and temporal dimensions to resolve motion fragmentation, achieving accuracy improvement without additional computational cost.
- **Novel neural architecture for egocentric event-based recognition:** The first end-to-end trainable framework specifically designed for gesture recognition from head-mounted event cameras, effective while maintaining computational efficiency.

2. Related Work

Next, we review related works on egocentric gesture recognition and event-based approaches to human perception. As shown in Table 1, our EgoEvGesture represents the first dataset for egocentric gesture recognition that uses real-world event streams, offering several advantages over existing RGB- or depth-based methods, as highlighted in the following sections.

2.1. Egocentric Gesture Recognition

Egocentric gesture recognition using RGB and depth sensors has been extensively explored [6, 17–22]. The EgoGesture dataset [7], one of the largest benchmarks, contains 83 gesture classes designed for wearable device interactions, which inspired our motion design. The EPIC-KITCHENS dataset [23] focuses on action classification in kitchen environments, but prioritizes general activities over specific gestures. The FPHA dataset [24] pioneered 3D hand pose annotations in egocentric scenarios but suffers from magnetic sensor interference and lacks two-hand pose data. The H2O dataset [25] is the first dataset to emphasize bimanual object interactions and achieves high precision in gesture recognition. However, it primarily relies on static image annotations, and lacks continuous dynamic gesture capture, which limits its applicability to real-time gesture recognition. Assembly101 [26] and ARCTIC [27] extend the scope of egocentric hand-object interaction datasets. While Assembly101 provides multi-view videos for activity understanding, its focus on assembly tasks restricts gesture diversity. ARCTIC offers dexterous bimanual manipulation data but lacks dynamic gesture annotations. HOI4D [28] introduces category-level human-object interaction labels, including panoptic segmentation, motion segmentation, and reconstructed 3D meshes, yet it only addresses single-hand manipulation tasks.

Traditional gesture recognition methods, such as SVM [29, 30], Random Forests [31], KNN [32, 33], and HMM [34, 35], rely on handcrafted features (e.g., optical flow, edge descriptors) to model gesture dynamics. These approaches are susceptible to noise in complex environments and struggle to capture subtle motion variations, resulting in degraded performance for fast or intricate gestures. Deep learning has become the mainstream for gesture recognition. 2D CNNs [36, 37] extract spatial features from single frames, whereas 3D CNNs [38, 39] capture short-term spatiotemporal dependencies. However, single CNN models often fail to balance global and local feature interactions in egocentric scenarios. RNNs [40, 41] model temporal relationships but face challenges such as vanishing gradients and inefficiency in long-sequence processing. Transformers [42–44] excel at capturing long-range temporal dependencies and demonstrate potential, though their efficiency in real-time applications remains unresolved. Existing methods often modify base network architectures to improve performance. For instance, the Temporal Segment Network (TSN) [45] divides videos into segments for feature extraction and classification, effectively capturing temporal dynamics. This approach has been applied to action classification in the Assembly101 dataset, demonstrating advantages in modeling temporal information.

Despite progress, RGB/depth-based methods remain constrained by motion blur, high power consumption, and limited dynamic capture capabilities, particularly in fast-moving or low-light conditions. These limitations have spurred the adoption of event cameras, which offer high temporal resolution and robustness to motion blur, opening new opportunities for gesture recognition.

2.2. Event-based Methods for Human Perception

Event cameras, inspired by biological vision systems, asynchronously record pixel intensity changes, making them highly suitable for dynamic scenes with fast motion [10, 12, 46]. Recent works have explored the use of event cameras for human perception tasks such as human pose estimation [16, 47–49], action classification [50, 51], eye tracking [52–55], sign language [56, 57] and head pose estimation [58], demonstrating their advantages in temporal resolution and robustness to motion blur. All existing event-based studies on hand motion analysis are conducted from a third-person perspective. DVS128 [1] proposed the first event-based hardware system for gesture recognition, achieving high accuracy and low latency under low-power conditions for gesture recognition. However, this system faces challenges such as low resolution and a lack of hand pose diversity. EventHands [13] achieves 1kHz 3D hand pose estimation using event cameras, which leverages Locally Normalized Event Surfaces (LNES) to aggregate asynchronous event data into a compact 2D representation, emphasizing temporal locality and enabling efficient real-time processing with high accuracy. This method has been widely applied in the field of human body perception [16, 59], achieving excellent results. EvHandPose [60] employs a novel hand flow representation and a weakly-supervised framework to address motion ambiguities in event streams, though its focus lies in reconstruction rather than gesture recognition. Ev2Hands [61] achieved the first 3D tracking of two fast-moving and interacting hands from a single monocular event camera. EHoa [62] pioneered hand-object action recognition via event vision. EvRGBHand [63] introduced complementary use of event streams and RGB frames for hand mesh reconstruction. E2(GO)MOTION [64] synthesized the N-EPIC-Kitchens dataset, the first egocentric action recognition dataset based on event data. Their work highlights the potential of event data for action recognition, particularly excelling in scenarios with rapid motion and low lighting. The recent work Helios [59] proposes an event-based gesture recognition system optimized for smart eyewear. The study introduces a synthetic event dataset with seven gesture classes to train the recognition model, showcasing the potential for low-power, real-time implementation in wearable devices. However, the system exhibits notable accuracy degradation in real-world testing compared to synthetic data performance, and the restricted gesture taxonomy limits its generalizability. Meanwhile, the authors do not address the open-source accessibility of the dataset. However, reliance on synthetic data introduces challenges due to the real-synthetic domain gap.

The unique asynchronous and sparse nature of event data creates inherent incompatibilities with conventional RGB-based processing paradigms, which are designed for synchronous frame-based inputs. While event streams offer microsecond temporal resolution and sparse asynchronous encoding of luminance changes, their ultra-high temporal granularity introduces unique computational challenges. Existing event-based approaches predominantly focus on instantaneous feature extraction tasks (e.g., 3D keypoint estimation) rather than continuous temporal understanding. This limitation stems from two inherent properties: (1) The asynchronous discrete nature of event representation complicates the modeling of coherent temporal dynamics, and (2) The fragmented temporal cues inherent in sparse event streams hinder process-level semantic interpretation. Consequently, current methodologies struggle to reconcile the conflict between leveraging fine-grained motion dynamics captured by event sensing and establishing holistic temporal reasoning frameworks. This modality discrepancy underscores the critical need for dedicated architectures addressing temporal continuity in event-based gesture recognition.

A comprehensive comparison of existing gesture recognition datasets across modalities is presented in Table 1. The table systematically evaluates 18 datasets through eight critical dimensions: sensing modality, data volume, action classes, two-hand interaction support, spatial resolution, publication year, real-world applicability, and first-person perspective. Notably, EgoEvGesture (our proposed dataset) establishes four key advantages: (1) First and only event-based dataset for egocentric gestures – Existing event datasets focus on third-person actions, while ours captures head-motion-contaminated events unique to first-person view. (2) the largest event-based sample volume (5,419 samples), (3) the richest gesture vocabulary among event-based datasets (38 classes), and (4) native support for two-hand interaction in egocentric scenarios - features previously unavailable in existing event-stream benchmarks.

3. EgoEvGesture Dataset

3.1. Head-Mounted Capture System

Our egocentric gesture acquisition platform (illustrated in Figure 1a) employs a custom-designed head-mounted system (HMS) comprising a lightweight bicycle helmet modified with 3D-printed mounts to rigidly affix two Prophesee EVK4 event cameras and an Intel RealSense D435 depth camera. Temporal synchronization between event streams and RGB-D frames is achieved through hardware triggering, where the Intel RealSense D435 emits a synchronization signal to align data acquisition across all sensors. The event cameras utilize 4 mm focal length lenses (MV-LD-4-4M-G) providing a 94° horizontal field of view (FOV) with a native resolution of 1280 × 720 pixels. Each pixel has a size of $4.86\mu\text{m} \times 4.86\mu\text{m}$ with temporal resolution up to 1 MHz, capturing brightness changes through asynchronous events. For normal light conditions, we employed the default EVK4 threshold configuration (0% bias_diff_off and 0% bias_diff_on). In low-light scenarios, sensitivity was enhanced by configuring 20% bias_diff_off and 20% bias_diff_on parameters to increase event generation rate. The Intel RealSense D435 RGB-D camera operates at 30 fps with synchronized 1280 × 720 resolution for depth streams, which may be used for further research. The system connects via USB 3.0 to a host computer for power delivery and real-time data streaming, enabling uninterrupted recording sessions. The compact design and flexible head-mounted system (HMS) allow users to freely move their heads and perform hand movements while ensuring precise temporal alignment.

Table 1. A comprehensive comparison of relative datasets including details on their modalities, volumes, action classes, two-hand interaction presence, resolutions, years of publication, real-world applicability, and first-person perspective availability.

Dataset	Modality	Volume	Clss	2H	Res	Vr	Real	1st-P
Ego-Gesture [7]	RGB	3M	83	✓	640p	18	✓	✓
FPHA [24]	RGB	0.1M	45	✗	1080p	18	✓	✓
EPIC-KITCHENS [23]	RGB	11.5M	149	✓	1080p	18	✓	✓
H20 [25]	RGB	0.57M	36	✓	720p	21	✓	✓
Assembly101 [26]	RGB	110M	1380	✗	1080p	21	✓	✓
ARCTIC [27]	RGB	2.1M	11	✓	2.8k	24	✓	✓
HOI4D [28]	RGB	2.4M	54	✗	8k	24	✓	✓
DVS128 [1]	Event	1342S	10	✗	128 ²	17	✓	✗
N-EPIC [64]	Event	NA	8	✓	225 ²	22	✗	✓
EHoA [62]	E+R	2144S	8	✗	346p	24	✓	✗
EvRealHands [60]	E+R	79m	NA	✗	720p	23	✓	✗
Ev2Hands-S [61]	Event	*	NA	✓	512 ²	23	✗	✗
Ev2Hands-R [61]	E+R	20m	NA	✓	346 ²	23	✓	✗
EventHands [13]	Event	100h	NA	✗	240p	21	✗	✗
EventEgo3D [16]	Event	127m	NA	✗	320 ²	24	Both	✓
Helios [59]	Event	600S	7	✗	320 ²	24	✓	✓
EVREALHANDS [63]	E+R	74m	NA	✗	346p	24	✓	✗
EgoEvGesture (Ours)	Event	5419S	38	✓	720p	25	✓	✓

✓ = Yes ✗ = No **Abbreviations:** “E+R” denotes Event+RGB, “2H” denotes Two-Hand Interaction, “Clss” denotes Classes, “NA” denotes Not Available

Units: “M” denotes Million, “S” denotes Samples, “m” denotes minutes, “h” denotes Hours, * denotes Number of events (3.12×10^8)



(a) Proposed head-mounted capture system.



(b) Recording environment.

Fig. 1. (a) Proposed head-mounted capture system. It integrates two Prophesee EVK4 event cameras (left/right) and an Intel RealSense D435 RGB-D sensor (center). (b) Recording environment. Each participant is equipped with the HMS and performed a series of 38 distinct gestures under normal light and low light conditions.

3.2. Data Collection Protocol

The dataset consists of data from 10 participants, encompassing a diverse range of body types and genders. Each participant is equipped with the HMS and performed a series of 38 distinct gestures (as illustrated in Figure 2) under both normal and low-light conditions (as illustrated in Figure 1b). Each gesture is executed at least four times by each participant, ensuring a robust and varied dataset. The gestures are categorized into three main groups:

- **Single-Hand Gestures (Right Hand):** 11 classes including Wave to the right, Wave to the left, Right thumb points to the right, Right index finger points to the left, Tap, Spread, Shrink, Swipe, Draw a circle, Draw an X, NO (Shake finger).

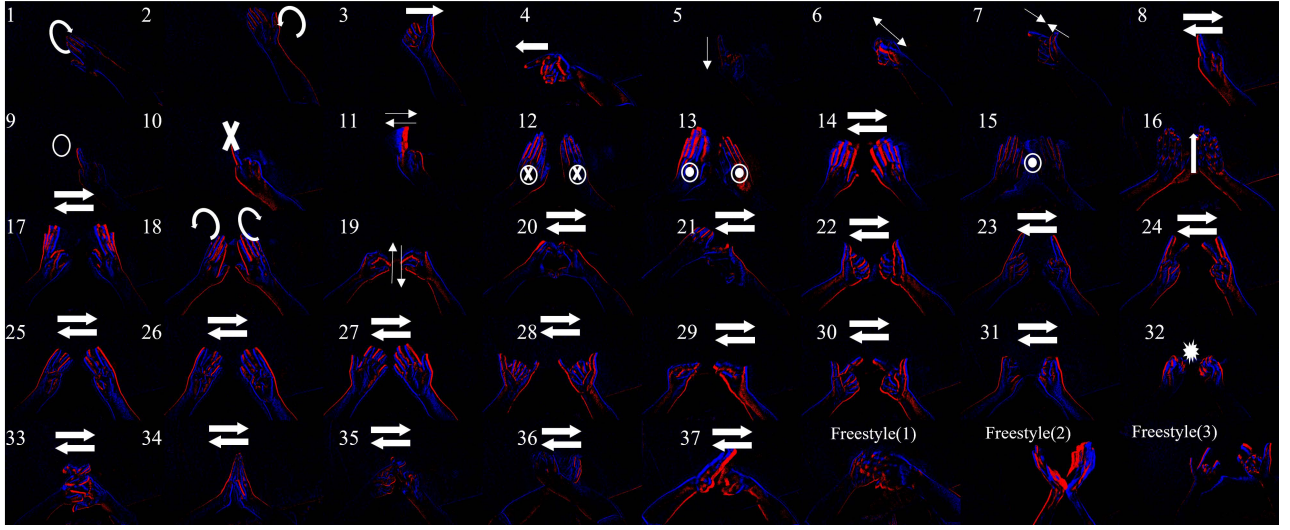


Fig. 2. The 38 classes of hand gesture designed in our proposed EgoEvGesture dataset. The figure shows events represented by LNES, with arrows indicating the direction of hand (thick arrows) or finger (thin arrows) movements. The freestyle motions vary among participants, with three examples shown in the figure.

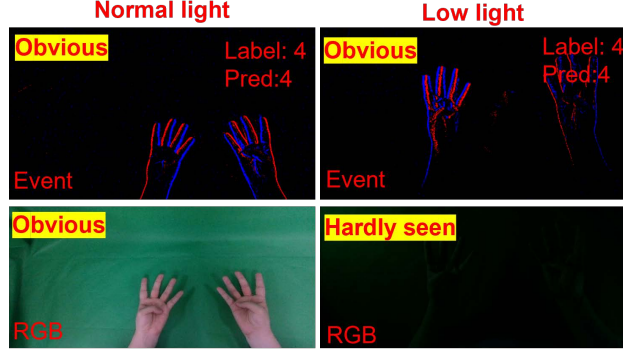


Fig. 3. A comparison of what an event camera (top) and an RGB camera (bottom) captured under normal light (left) and low light (right) conditions. Event cameras are almost unaffected by lighting conditions, while RGB images are barely distinguishable in low light conditions.

- **Two-Hand Gestures (No Occlusion):** 21 classes including Wave down, Wave up, Wave normally (arms close and move away), Raise arms, Push forward, OK, Flip palms, Grab, Make a heart, Camera gesture, Thumbs up, Show number 1-9, Make a fist.
- **Two-Hand Gestures (Mutual Occlusion):** 6 classes emphasizing challenging hand-hand interactions including Interlock fingers, Clap hands, Cross index fingers, Rotate arms, Salute with a fist, Freestyle motion.

Each participant performed all gestures under controlled normal illumination and low light conditions, with at least four repetitions per gesture-condition combination. Figure 3 contrasts the outputs of RGB and event cameras across lighting regimes, demonstrating the robustness of the latter to illumination variations.

3.3. Dataset Composition and Statistics

The dataset provides 5,419 finely segmented event data (~193 GB) with corresponding labels based on the precise start and end times of each action. The duration of each gesture performed by different participants is depicted in Figure 4, reflecting personalized articulation speeds. The dataset is characterized by its high variability as shown in Figure 5, which uses different normalized time event rates to reveal three fundamental characteristics through vertically stacked visualizations, including different people performing different actions event rates, different people's average event rates across all actions in different environments, and event rates for unilateral and bilateral actions. Figure 5(a) shows a clear difference in event rates when each subject performs different actions, with a nearly 10 \times difference between the simplest action and the most complex gesture, demonstrating the distinctiveness of the action design. Figure 5(b) shows a clear difference in average event rates between different subjects, regardless of whether it is normal light or low light. Figure 5(c)

Duration per Action by Subject

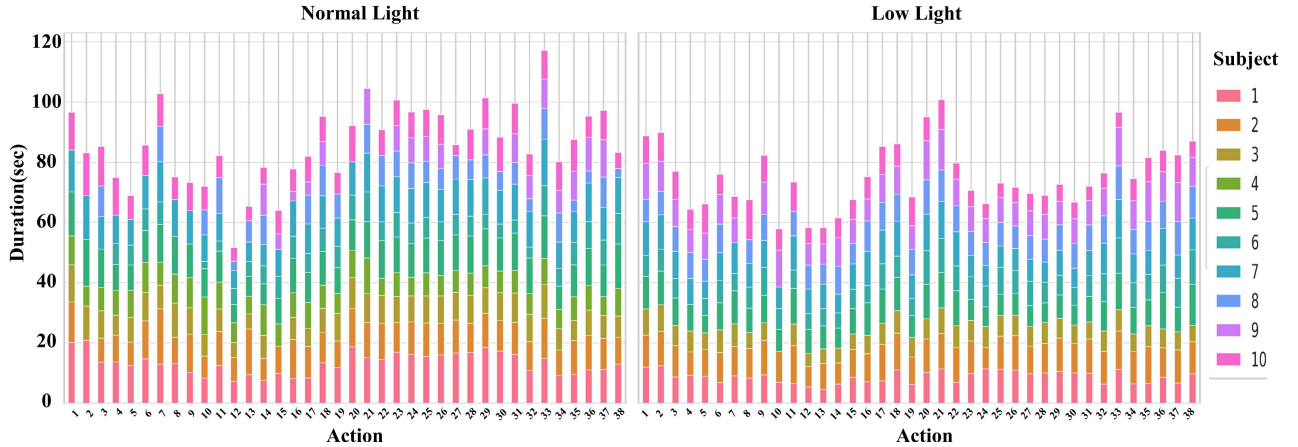


Fig. 4. Action duration distributions across subjects under normal light (left) and low light (right) conditions. Each vertical bar represents cumulative duration for a specific action, with colored segments indicating subject-wise contributions.

shows that the event rate for bilateral actions is significantly higher than that for unilateral actions, demonstrating the difference between the two types of actions. This variability is crucial for training robust gesture recognition models that can generalize across different users and lighting conditions. The inclusion of event camera data, which is less sensitive to lighting variations compared to traditional RGB cameras, further enhances the dataset’s utility for research in challenging environments.

In summary, the EgoEvGesture dataset offers a rich and diverse collection of egocentric gesture data, captured under varying lighting conditions, making it a valuable resource for advancing research in gesture recognition using event cameras.

4. Methodology

4.1. Architecture Overview: Dual-Motion Disentanglement Framework

To address the critical challenge of ego-hand motion entanglement in event streams while capturing holistic temporal patterns, we propose a temporal pyramid architecture with three progressive processing stages (Fig. 6):

We first convert raw events into Locally Normalized Event Surfaces (LNES) that focus on the most recent temporal signature to suppress historical ego-motion artifacts while maintaining real-time performance. We then adopt Blaze & VMamba blocks to extract spatiotemporal features. Our Blaze encoder-decoder, adapted from [14] with proven efficiency in human-centric perception [16], processes each temporal bin. The VMamba block addresses sparse event processing and long-term temporal modeling through discrete state space equations (detailed in Sec. 4.2). Finally, we employ the Bidirectional temporal shift module (BTSM) to resolve temporal semantic fragmentation caused by segmented processing and perform temporal alignment (detailed in Sec. 4.3).

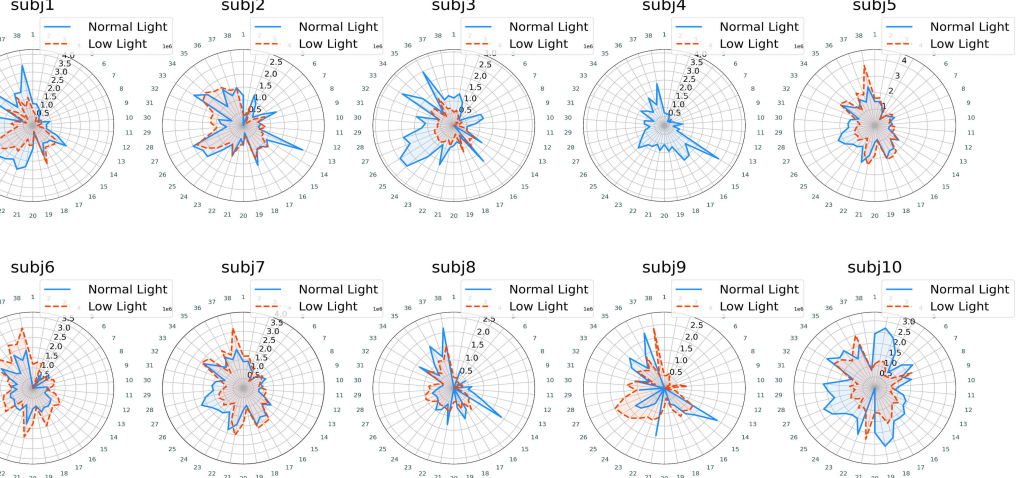
4.2. VMamba Block

Despite the ability to adapt to high dynamic ranges, event-based gesture recognition faces challenges due to the sparsity of events, which makes it difficult for traditional methods to effectively focus on key areas. Meanwhile, the very high event resolution, while enhancing the ability to capture fine details, also makes long-term temporal understanding more challenging. To address the aforementioned challenges, we introduce the VMamba block, which addresses this modality discrepancy through adaptive temporal continuity - maintaining feature dimensions (for compatibility) while implementing dynamic state transitions. Our design philosophy centers on selective computation focusing - preserving computational resources for active temporal regions without sacrificing temporal granularity. The VMamba block operates as follows:

$$\begin{aligned}
 \Delta_t &= \text{softplus}(\mathbf{W}_\Delta \mathbf{x}_t + \mathbf{b}_\Delta) \quad (\text{Time-aware gating}), \\
 (\mathbf{B}_t, \mathbf{C}_t) &= \text{split}(\mathbf{W}_B \mathbf{C} \mathbf{x}_t) \quad (\text{Input/Output projection}), \\
 \tilde{\mathbf{A}}_t &= \exp(\Delta_t \mathbf{A}) \quad (\text{Continuous-discrete conversion}), \\
 \tilde{\mathbf{B}}_t &= \Delta_t \mathbf{B}_t \quad (\text{Sparsity modulation}), \\
 \mathbf{h}_t &= \tilde{\mathbf{A}}_t \mathbf{h}_t - 1 + \tilde{\mathbf{B}}_t \odot \mathbf{x}_t \quad (\text{Selective memory}), \\
 \mathbf{y}_t &= \mathbf{C}_t \mathbf{h}_t + \mathbf{D} \odot \mathbf{x}_t \quad (\text{Residual learning}),
 \end{aligned} \tag{1}$$

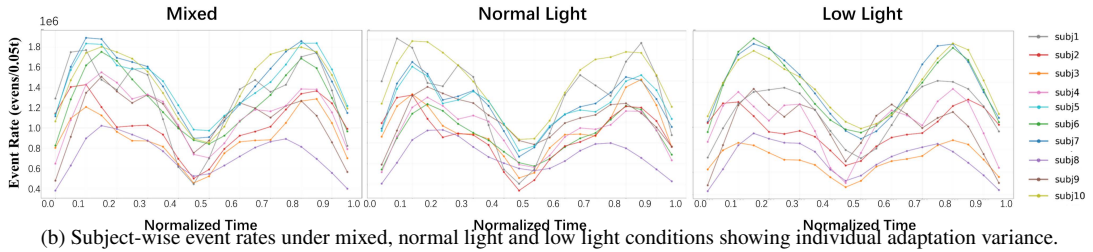
where: - Δ_t is computed via a time-aware gating mechanism, adaptively controlling temporal dependencies. - \mathbf{B}_t and \mathbf{C}_t are obtained through input/output projection, modulating input sparsity and serving as linear transformations. - $\tilde{\mathbf{A}}_t$ bridges

Average Event Rate per Action per Subject



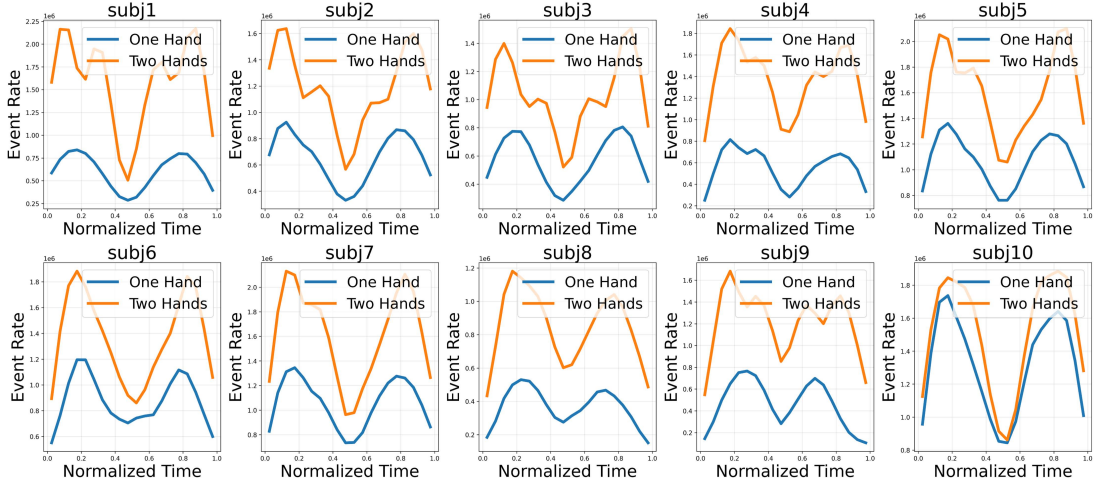
(a) Average action event rates under normal light and low light conditions across 10 subjects. Each subplot represents data from a single subject, with 38 discrete actions uniformly distributed around the 360° axis. Higher variance in complex gestures indicates movement pattern diversity.

Average Event Rate by Subject



(b) Subject-wise event rates under mixed, normal light and low light conditions showing individual adaptation variance.

Comparison of Event Rates between One-Hand and Two-Hands



(c) Bimanual vs unimanual event rates. Higher event density in two-hand gestures confirms asymmetric motion dynamics.

Fig. 5. Comprehensive event rate statistics: (a) Action-class variability; (b) Subject-specific patterns across lighting conditions; (c) Handedness effects.

continuous-time dynamics and discrete-time updates. - $\tilde{\mathbf{B}}_t$ amplifies or reduces input features based on temporal relevance. - \mathbf{h}_t updates the hidden state through selective memory, combining temporal state propagation and sparsity-aware input integration. - \mathbf{y}_t combines transformed hidden states with residual input connections for stable training.

The VMamba block offers three key advantages:

- **Plug-and-Play Compatibility:** Maintains original feature dimensions through dimension-preserving operations, enabling seamless integration into existing architectures.
- **Sparse Event Adaptation:** Selectively focuses computation on active temporal regions through adaptive temporal attention, effectively handling sparse event patterns.

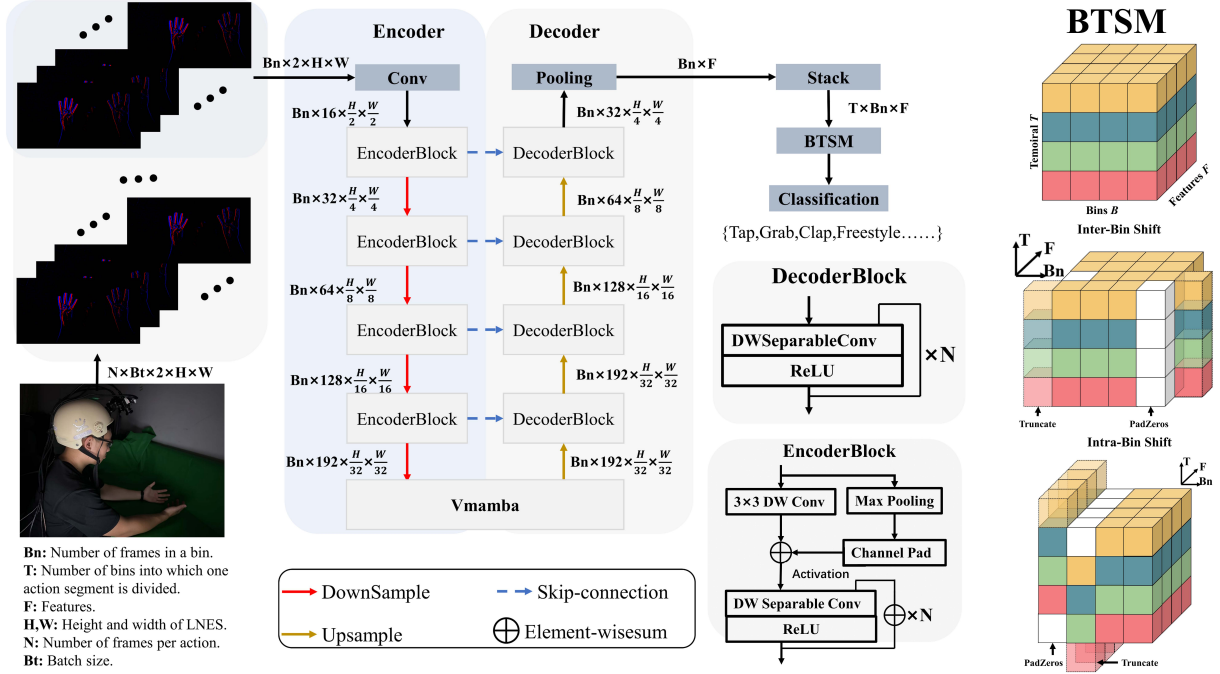


Fig. 6. Three-stage processing pipeline: (1) LNES converts raw events to normalized surfaces preserving recent temporal signatures (2) Blaze & VMamba blocks extract multi-scale features (3) BTSM aligns temporal context

- **Linear Complexity Scaling:** Achieves efficient computation with $O(N^2 + NF)$ complexity, where N denotes the number of temporal steps and F represents the feature dimension. The NF term specifically captures the linear scaling of feature transformation costs across temporal windows, enabling practical processing of long videos.

4.3. Bins-Temporal Shift Module (BTSM)

Existing event-based approaches predominantly focus on instantaneous feature extraction tasks (e.g., 3D keypoint estimation) rather than continuous temporal understanding. This limitation arises from two key properties: (1) the asynchronous discrete nature of event representation complicates the modeling of coherent temporal dynamics, and (2) the fragmented temporal cues inherent in sparse event streams hinder process-level semantic interpretation. Consequently, current methodologies struggle to reconcile the conflict between leveraging fine-grained motion dynamics captured by event sensing and establishing holistic temporal reasoning frameworks. This modality discrepancy underscores the critical need for dedicated architectures addressing temporal continuity in event-based gesture recognition. To tackle these challenges, the Bins-Temporal Shift Module (BTSM) implements dual-stage temporal modeling through cascaded shift operations including Intra-Bin Fusion and Inter-Bin Fusion. This parameter-free design enables comprehensive temporal modeling through layered feature propagation and addresses temporal semantic fragmentation caused by segmented processing.

4.3.1. Intra-Bin Fusion

The intra-bin fusion stage processes temporal relationships within each segment via channel-wise shifting, where $\frac{F}{4}$ channels are shifted left/right along temporal dimension within bins, preserving spatial locality. Given input features $X \in \mathbb{R}^{Bt \times T \times Bn \times F}$ where Bt =batch size, T =number of bins into which one action segment is divided, Bn =number of frames in a bin, and F =features, the module operates as follows:

$$X_{intra} = \mathcal{T}_{local}(X) = \begin{cases} X^{left} = \text{roll}(X_{:, :, :, 0:\frac{F}{4}}, \text{shift} = -1, \text{dim} = 2), \\ X^{right} = \text{roll}(X_{:, :, :, \frac{F}{4}:\frac{F}{2}}, \text{shift} = +1, \text{dim} = 2), \\ X^{static} = X_{:, :, :, \frac{F}{2}:}, \end{cases} \quad (2)$$

$$X_{intra} = \text{concat}(X^{left}, X^{right}, X^{static}) \in \mathbb{R}^{Bt \times T \times Bn \times F}, \quad (3)$$

where:

- $\text{roll}(X, \text{shift}, \text{dim})$: A function that shifts the elements of X along the specified dimension dim by the amount shift . A negative shift moves elements to the left, while a positive shift moves elements to the right.
- X^{left} : The left-shifted features, obtained by shifting the first $\frac{F}{4}$ channels to the left along the temporal dimension.

- X^{right} : The right-shifted features, obtained by shifting the next $\frac{F}{4}$ channels to the right along the temporal dimension.
- X^{static} : The remaining $\frac{F}{2}$ channels that are not shifted, representing static features.
- concat: A function that concatenates the shifted and static features along the feature dimension.

4.3.2. Inter-Bin Fusion

The Inter-Bin Fusion stage models cross-segment dependencies through bin-axis shifting. This operation implements cross-bin feature propagation while maintaining temporal ordering within bins, enabling the modeling of long-range temporal dependencies. The module operates as follows:

$$\tilde{X} = X_{intra} \in \mathbb{R}^{Bt \times T \times Bn \times F}, \quad (4)$$

$$X_{inter} = \mathcal{T}_{inter}(\tilde{X}) = \begin{cases} \tilde{X}^{left} = \text{roll}(\tilde{X}_{:,:,0:\frac{F}{4}}, \text{shift} = -1, \text{dim} = 1), \\ \tilde{X}^{right} = \text{roll}(\tilde{X}_{:,:,\frac{F}{4}:\frac{F}{2}}, \text{shift} = +1, \text{dim} = 1), \\ \tilde{X}^{static} = \tilde{X}_{:,:,\frac{F}{2}:}, \end{cases} \quad (5)$$

$$X_{final} = \text{concat}(\tilde{X}^{left}, \tilde{X}^{right}, \tilde{X}^{static}) \in \mathbb{R}^{Bt \times T \times Bn \times F}, \quad (6)$$

where:

- \tilde{X} : The input features to the Inter-Bin Fusion stage, which are the output features from the Intra-Bin Fusion stage. It has the same dimension as X_{intra} , i.e., $\mathbb{R}^{Bt \times T \times Bn \times F}$.
- X_{inter} : The intermediate features after applying the bin-axis shifting operation. It is a tuple containing the left-shifted, right-shifted, and static features along the bin axis.
- \tilde{X}^{left} : The left-shifted features along the bin axis, obtained by shifting the first $\frac{F}{4}$ channels to the left along the bin dimension (dim=1).
- \tilde{X}^{right} : The right-shifted features along the bin axis, obtained by shifting the next $\frac{F}{4}$ channels to the right along the bin dimension (dim=1).
- \tilde{X}^{static} : The remaining $\frac{F}{2}$ channels that are not shifted along the bin axis, representing static features.
- X_{final} : The final output features after concatenating the shifted and static features along the feature dimension. It has the same dimension as the input features \tilde{X} , i.e., $\mathbb{R}^{Bt \times T \times Bn \times F}$.
- $\text{roll}(X, \text{shift}, \text{dim})$ and concat : Same as in the Intra-Bin Fusion stage.

4.3.3. Mechanism Analysis

The dual-shift design establishes:

- **Local Connectivity**: The intra-bin shift operation captures short-term motion patterns with fine temporal granularity, ensuring that local temporal dynamics are effectively modeled.
- **Global Context**: The inter-bin shift operation propagates features across distant segments, enabling the capture of long-range temporal dependencies and holistic temporal understanding.
- **Channel-Specific Dynamics**: 50% channels ($\frac{F}{2}$) remain unshifted to preserve spatial semantics, ensuring that the spatial context is not lost during the temporal modeling process.

This design choice allows the BTSM to reconcile the fine-grained motion dynamics captured by event sensing with the need for holistic temporal reasoning, making it particularly effective for event-based gesture recognition tasks. The module's parameter-free nature and lightweight computation make it a practical solution for real-world applications.

4.4. Loss Function

We employ standard cross-entropy loss for gesture classification:

$$\mathcal{L} = - \sum_{c=1}^C y_c \log(p_c), \quad (7)$$

where y_c denotes ground-truth labels and p_c represents predicted class probabilities.

5. Experiments

5.1. Dataset Configuration and Evaluation Protocol

Our data splitting methodology focuses on two distinct evaluation dimensions: illumination robustness evaluation and two different training-test split methods, the heterogeneous split and the homogeneous split.

5.1.1. Illumination Robustness Validation Split

To evaluate the robustness of our method under different illumination, we consider three testing scenarios for each of the 3 splits:

- **Normal light condition only:** This scenario tests the model’s performance under normal light conditions, serving as a baseline to compare with other scenarios.
- **Low light condition only:** Here, we assess how the model handles low light conditions, which are more challenging due to reduced visibility and altered appearance of pedestrians.
- **Mixed condition:** This scenario combines both normal and low light conditions, simulating real-world situations where the model may encounter a variety of lighting conditions within the same test set.

5.1.2. Two Different Training-Test Split Methods

We implement two evaluation protocols: heterogeneous split (heter) and homogeneous split (homo).

- **Heterogeneous Split:** In heterogeneous split, we divide the dataset by subjects. The test set consists of all data from subjects 1, 2, and 9, while the training set is composed of data from the remaining 7 subjects. This design simulates a real-world scenario where the model encounters previously unseen subjects under various illumination conditions, evaluating the model’s generalization ability across different identities and lighting environments. By keeping the test subjects completely separate from the training subjects, we can ensure that the model can perform well on diverse data and avoid overfitting to specific subjects.
- **Homogeneous Split:** Unlike the heterogeneous split, the homogeneous split maintains identity consistency under different illumination conditions. For each subject, we divide their sequences into three daytime/low-light sequences for training and one for validation. This design evaluates the model’s ability to handle variations of the same identity under different lighting conditions. By keeping the same subjects in both the training and validation sets, we can assess the model’s adaptability to different illuminations for known identities. Furthermore, this homogeneous split protocol validates the effectiveness of the compared methods under simpler conditions (where data similarity is high). By contrasting it with the heterogeneous split, we demonstrate that data diversity poses a greater challenge for different methods. Through comparative experimental results, we further illustrate the effectiveness of our proposed method.

5.2. Main Results on Proprietary Dataset

Figure 7 presents the normalized confusion matrix for our proposed method testing in the Heter split. The diagonal elements represent correct classifications, while off-diagonal entries indicate misclassifications. Our model demonstrates strong discriminative capabilities, particularly in waving and numbers, achieving classification accuracies above 90%. Notable misclassifications occur primarily in freestyle motions, likely attributed to high inter-personal variability in movement execution and the test set containing completely unseen movement patterns that differ significantly from training data distributions. Other confusion occurs mainly between visually similar activities like Push forward (class 15) and Wave up (class 12) or Raise arms (class 14). All experiments are conducted on a single A100 GPU using the AdamW optimizer with a learning rate of 1×10^{-4} , trained for 60 epochs with early stopping to prevent overfitting.

5.3. Comparative Methods and Results

We conduct comprehensive comparisons with four approaches that address distinct aspects of vision-based action recognition particularly relevant to action recognition under varying conditions.

- **STLLer** [65]: A spiking neural network (SNN) designed for event-based action recognition, utilizing spatiotemporally aware life-long learning. This method is noted for its ability to learn continuously, adapting to new actions over time. This biologically-inspired approach achieves state-of-the-art performance on the DVS128 dataset.
- **Assembly** [45]: A strong baseline derived from the AssemblyHands dataset, originally designed for RGB-based action recognition using ResNet-101 backbone.
- **EventEgo3D** [16]: The first framework addressing egocentric 3D perception tasks with event cameras, combining LNES event representation with efficient BlazeBlocks for spatial-temporal feature extraction, marking it as a pioneer in egocentric event understanding. Given its strong alignment with our task requirements, we select it as our baseline method.

Confusion Matrix (%)

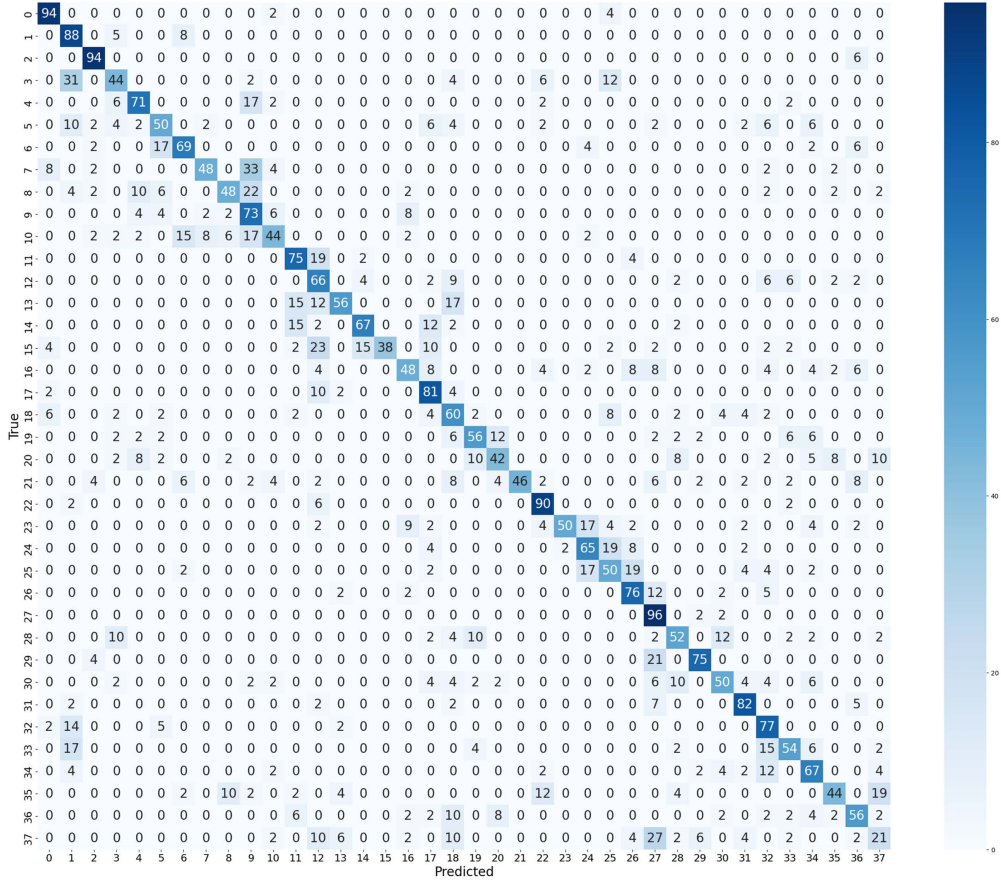


Fig. 7. Confusion matrix for mixed-condition testing in Heter split using our method. Diagonal entries represent recall rates for 38 activity classes, while off-diagonal values show common misclassifications.

- **EventPoint** [49]: A point cloud approach for event data processing that achieves competitive performance on the DHP19 dataset with low computational overhead.

Table 2. Cross-Method Performance Comparison (Accuracy %).

Method	Heter Split		Homo Split		Params (M)
	Mixed	Day/Night	Mixed	Day/Night	
S-tllr [65]	30.2	28.4/27.9	50.0	49.7/50.1	13.96
Assembly [45]	59.6	59.8/58.6	98.9	98.9/98.9	42.72
EventEgo3D [16]	36.4	39.5/38.3	97.4	97.8/97.2	6.50
EventPoint [49]	30.0	29.3/28.1	98.6	98.4/98.7	3.35
Ours	62.7	62.8/62.5	99.1	99.2/98.9	7.01

* *EventEgo3D*: Originally designed for 3D keypoint estimation. We adapt its feature extractor with our classification head.

Table 2 presents the performance comparison across different methods. Our method achieves the best performance in both Heterogeneous and Homogeneous splits. For the Heterogeneous Split, our method achieves 62.7% accuracy on the Mixed-condition test, significantly outperforming other methods such as STLLer (30.2%), Assembly (59.6%), EventEgo3D (36.4%), and EventPoint (30.0%). Consistent normal light/ low light performance (62.8% day vs 62.5% night) demonstrates illumination robustness. All methods except S-tllr achieve an accuracy higher than 97% in the homo split validating experimental consistency. The parameter count of our model is 7.01M, which is relatively small, indicating that our model is

efficient and effective for event-based egocentric action gesture recognition. In conclusion, our method outperforms existing approaches in action recognition under varying conditions while maintaining a relatively small number of parameters, demonstrating its robustness and effectiveness.

5.4. Component Ablation Analysis

As shown in Table 3, our ablation study reveals the effectiveness of different modules. The baseline model achieves 36.4% accuracy on the Heterogeneous Mixed testing set. Introducing the BTSM boosts the accuracy to 58.1%, demonstrating the importance of temporal information in action recognition. Adding the Visual Mamba module alone improves the accuracy to 45.3%, indicating the value of spatial feature extraction. The full model combining TSM and VMamba achieves the highest accuracy of 62.7%, showing that both modules contribute significantly to performance enhancement.

Table 3. Module Contribution in Heter Mixed Testing (%).

Configuration	Mixed Accuracy
Baseline	36.4
+BTSM only	58.1 (+21.7)
+VMamba only	45.3 (+8.9)
Full Model	62.7 (+26.3)

5.5. Quantitatively Result on DVS128 Gesture

To validate the generalization capability of our proposed architecture beyond our proprietary dataset, we conduct extensive experiments on the widely recognized event-based gesture recognition benchmark, DVS128 Gesture [1]. This dataset consists of 1,342 instances of 11 distinct hand gestures captured using dynamic vision sensors, presenting unique challenges in sparse temporal feature learning. As shown in Table 4, our approach achieves a remarkable accuracy of 97.0% on this benchmark, demonstrating its strong generalization capability. This result matches the accuracy of 97.0% obtained through reimplementation of the open source state-of-the-art approach S-tllr [65] without access to its pre-trained models, despite their reported accuracy of 97.7%. For S-tllr, we follow the settings described in its official implementation. For all other methods, experiments are conducted on a single A100 GPU using the AdamW optimizer with a learning rate of 1×10^{-4} , trained for 60 epochs with early stopping to prevent overfitting.

Table 4. Performance comparison on DVS128 Gesture benchmark. Our method achieves state-of-the-art accuracy without pretrained models, outperforming the reimplemented state-of-the-art S-tllr and other methods. Results highlight robustness to temporal sparsity and gesture variability. * denotes our reimplementation.

Method	Accuracy (%)
Assembly [45]	91.3
EventEgo3D [16]	81.8
EventPoint [49]	76.1
S-tllr [65]*	97.0
Ours	97.0

The competitive performance on DVS128 Gesture can be attributed to several factors inherent in our proposed architecture. First, our lightweight CNN with asymmetric depthwise convolutions effectively reduces parameters while preserving spatiotemporal features, which is crucial for handling the sparse and asynchronous nature of event-based data. This design choice not only enhances computational efficiency but also maintains the essential information needed for accurate gesture recognition. Second, the plug-and-play state-space model, acting as a context block, significantly enhances the model’s ability to filter out irrelevant motion patterns and helps focus on the actual gesture dynamics, thereby improving recognition accuracy. Third, the parameter-free Bins-Temporal Shift Module (BTSM) efficiently fuses sparse events by shifting features along bins and temporal dimensions. This mechanism is particularly beneficial for event-based data where information is spread sparsely across time and space. By effectively aggregating these sparse events, BTSM ensures that the model can capture the complete gesture patterns even from limited and dispersed event inputs. In summary, the remarkable accuracy

of 96.97% on the DVS128 Gesture dataset demonstrates the strong generalization capability of our proposed architecture. This result, comparable to the state-of-the-art S-tllr approach, highlights the effectiveness of our method in handling the unique challenges of event-based data. The detailed analysis of our architecture’s components provides insights into their contributions to the overall performance, further validating the robustness and competitiveness of our approach across diverse datasets.

6. Conclusion

In this work, we address the new problem, i.e., event-based egocentric gesture recognition based on egocentric event cameras, and we introduce all the necessary tools required to address fundamental challenges in designing the method. We propose an egocentric gesture recognition framework featuring a three-stage processing pipeline: First, raw event streams are converted into Locally Normalized Event Surfaces (LNES) to suppress ego-motion artifacts from head movements. Subsequently, a lightweight Blaze encoder-decoder combined with a VMamba module extracts spatiotemporal features, addressing event sparsity and long-term temporal modeling. Finally, a parameter-free BTSM achieves motion-invariant temporal alignment through bidirectional propagation. To address the data gap, we construct EgoEvGesture, the first large-scale egocentric event-based gesture dataset, containing 5,419 samples of 38 gesture classes (single/two-hand interactions) from 10 subjects under normal and low light conditions. Experiments demonstrate that our method achieves 62.7% accuracy in heterogeneous testing with only 7M parameters, outperforming state-of-the-art approaches by 3.1%, while maintaining stable performance. As this is the first work on the egocentric gesture recognition using event cameras, the open-source release of the dataset and code is expected to foster synergistic advancements in event vision and egocentric interaction research. In the future, we plan to enhance HMS to make it more lightweight. We will leverage depth cameras as ground truth to explore egocentric hand keypoint estimation based on event cameras, and then extend the relevant findings to outdoor environments.

References

1. A. Amir, B. Taba, D. Berg, *et al.*, “A low power, fully event-based gesture recognition system,” in *Proceedings of the IEEE conference on computer vision and pattern recognition*, (2017), pp. 7243–7252.
2. K. Gao, H. Zhang, X. Liu, *et al.*, “Challenges and solutions for vision-based hand gesture interpretation: A review,” *Comput. Vis. Image Underst.* p. 104095 (2024).
3. T. Woo, W. Park, W. Jeong, and J. Park, “A survey of deep learning methods and datasets for hand pose estimation from hand-object interaction images,” *Comput. & Graph.* **116**, 474–490 (2023).
4. A. Bandini and J. Zariffa, “Analysis of the hands in egocentric vision: A survey,” *IEEE transactions on pattern analysis machine intelligence* **45**, 6846–6866 (2020).
5. J. Qi, L. Ma, Z. Cui, and Y. Yu, “Computer vision-based hand gesture recognition for human-robot interaction: a review,” *Complex & Intell. Syst.* **10**, 1581–1606 (2024).
6. S. Han, B. Liu, R. Cabezas, *et al.*, “Megatrack: monochrome egocentric articulated hand-tracking for virtual reality,” *ACM Trans. on Graph. (ToG)* **39**, 87–1 (2020).
7. Y. Zhang, C. Cao, J. Cheng, and H. Lu, “Egogesture: a new dataset and benchmark for egocentric hand gesture recognition,” *IEEE Trans. on Multimed.* **20**, 1038–1050 (2018).
8. F. Mueller, D. Mehta, O. Sotnychenko, *et al.*, “Real-time hand tracking under occlusion from an egocentric rgb-d sensor,” in *Proceedings of the IEEE international conference on computer vision*, (2017), pp. 1154–1163.
9. C. Plizzari, G. Goletto, A. Furnari, *et al.*, “An outlook into the future of egocentric vision,” *Int. J. Comput. Vis.* **132**, 4880–4936 (2024).
10. G. Gallego, T. Delbrück, G. Orchard, *et al.*, “Event-based vision: A survey,” *IEEE transactions on pattern analysis machine intelligence* **44**, 154–180 (2020).
11. C. Lan, Z. Yin, A. Basu, and R. H. Chan, “Tracking fast by learning slow: An event-based speed adaptive hand tracker leveraging knowledge in rgb domain,” *arXiv preprint arXiv:2302.14430* (2023).
12. S. Lin, G. Zheng, Z. Wang, *et al.*, “Embodied neuromorphic synergy for lighting-robust machine vision to see in extreme bright,” *Nat. Commun.* **15**, 10781 (2024).
13. V. Rudnev, V. Golyanik, J. Wang, *et al.*, “Eventhands: Real-time neural 3d hand pose estimation from an event stream,” in *Proceedings of the IEEE/CVF international conference on computer vision*, (2021), pp. 12385–12395.
14. V. Bazarevsky, Y. Kartynnik, A. Vakunov, *et al.*, “Blazeface: Sub-millisecond neural face detection on mobile gpus,” *arXiv preprint arXiv:1907.05047* (2019).
15. A. Torres, “mamba.py: A simple, hackable and efficient mamba implementation in pure pytorch and mlx.” <https://github.com/alexndrTL/mamba.py> (2024).
16. C. Millerdurai, H. Akada, J. Wang, *et al.*, “Eventego3d: 3d human motion capture from egocentric event streams,” in *Proceedings of the IEEE/CVF Conference on Computer Vision and Pattern Recognition*, (2024), pp. 1186–1195.
17. M. S. Shamil, D. Chatterjee, F. Sener, *et al.*, “On the utility of 3d hand poses for action recognition,” in *European Conference on Computer Vision*, (Springer, 2024), pp. 436–454.
18. W. Mucha and M. Kampel, “In my perspective, in my hands: Accurate egocentric 2d hand pose and action recognition,” in *2024 IEEE 18th International Conference on Automatic Face and Gesture Recognition (FG)*, (IEEE, 2024), pp. 1–9.
19. Z. Fan, T. Ohkawa, L. Yang, *et al.*, “Benchmarks and challenges in pose estimation for egocentric hand interactions with objects,” in *European Conference on Computer Vision*, (Springer, 2024), pp. 428–448.
20. W. Mucha and M. Kampel, “Hands, objects, action! egocentric 2d hand-based action recognition,” in *International Conference on Computer Vision Systems*, (Springer, 2023), pp. 31–40.
21. Y. Wen, H. Pan, L. Yang, *et al.*, “Hierarchical temporal transformer for 3d hand pose estimation and action recognition from egocentric rgb videos,” in *Proceedings of the IEEE/CVF conference on computer vision and pattern recognition*, (2023), pp. 21243–21253.
22. W. Roh, S. H. Lee, W. J. Ryoo, *et al.*, “Functional hand type prior for 3d hand pose estimation and action recognition from egocentric view monocular videos.” in *BMVC*, (2023), p. 193.
23. D. Damen, H. Doughty, G. M. Farinella, *et al.*, “The epic-kitchens dataset: Collection, challenges and baselines,” *IEEE Trans. on Pattern Anal. Mach. Intell.* **43**, 4125–4141 (2020).

24. G. Garcia-Hernando, S. Yuan, S. Baek, and T.-K. Kim, "First-person hand action benchmark with rgb-d videos and 3d hand pose annotations," in *Proceedings of the IEEE conference on computer vision and pattern recognition*, (2018), pp. 409–419.

25. T. Kwon, B. Tekin, J. Stühmer, *et al.*, "H2o: Two hands manipulating objects for first person interaction recognition," in *Proceedings of the IEEE/CVF international conference on computer vision*, (2021), pp. 10138–10148.

26. F. Sener, D. Chatterjee, D. Shelepor, *et al.*, "Assembly101: A large-scale multi-view video dataset for understanding procedural activities," in *Proceedings of the IEEE/CVF Conference on Computer Vision and Pattern Recognition*, (2022), pp. 21096–21106.

27. Z. Fan, O. Taheri, D. Tzionas, *et al.*, "Arctic: A dataset for dexterous bimanual hand-object manipulation," in *Proceedings of the IEEE/CVF Conference on Computer Vision and Pattern Recognition*, (2023), pp. 12943–12954.

28. Y. Liu, Y. Liu, C. Jiang, *et al.*, "Hoi4d: A 4d egocentric dataset for category-level human-object interaction," in *Proceedings of the IEEE/CVF Conference on Computer Vision and Pattern Recognition*, (2022), pp. 21013–21022.

29. J. Li, C. Li, J. Han, *et al.*, "Robust hand gesture recognition using hog-9ulbp features and svm model," *Electronics* **11**, 988 (2022).

30. P. N. Huu and T. Phung Ngoc, "Hand gesture recognition algorithm using svm and hog model for control of robotic system," *J. Robotics* **2021**, 3986497 (2021).

31. Y. Xing, G. Di Caterina, and J. Soraghan, "A new spiking convolutional recurrent neural network (scrnn) with applications to event-based hand gesture recognition," *Front. neuroscience* **14**, 590164 (2020).

32. Y. Zhang, B. Yuan, Z. Yang, *et al.*, "Wi-nn: Human gesture recognition system based on weighted knn," *Appl. Sci.* **13**, 3743 (2023).

33. R. Nogales and M. Benalcázar, "Real-time hand gesture recognition using knn-dtw and leap motion controller," in *Conference on Information and Communication Technologies of Ecuador*, (Springer, 2020), pp. 91–103.

34. L. Zhang, Y. Zhang, L. Niu, *et al.*, "Hmm static hand gesture recognition based on combination of shape features and wavelet texture features," in *Wireless and Satellite Systems: 10th EAI International Conference, WiSATS 2019, Harbin, China, January 12–13, 2019, Proceedings, Part II 10*, (Springer, 2019), pp. 187–197.

35. Z. Yang, Y. Li, W. Chen, and Y. Zheng, "Dynamic hand gesture recognition using hidden markov models," in *2012 7th International Conference on Computer Science & Education (ICCSE)*, (IEEE, 2012), pp. 360–365.

36. J. Yu, M. Qin, and S. Zhou, "Dynamic gesture recognition based on 2d convolutional neural network and feature fusion," *Sci. Reports* **12**, 4345 (2022).

37. O. Köpüklü, A. Gunduz, N. Kose, and G. Rigoll, "Real-time hand gesture detection and classification using convolutional neural networks," in *2019 14th IEEE international conference on automatic face & gesture recognition (FG 2019)*, (IEEE, 2019), pp. 1–8.

38. H. Mansoor, N. Kalra, P. Goyal, *et al.*, "Hand gesture recognition using 3d cnn and computer interfacing," in *Inventive Systems and Control: Proceedings of ICISC 2022*, (Springer, 2022), pp. 727–736.

39. P. Molchanov, S. Gupta, K. Kim, and J. Kautz, "Hand gesture recognition with 3d convolutional neural networks," in *Proceedings of the IEEE conference on computer vision and pattern recognition workshops*, (2015), pp. 1–7.

40. S. Shin and W.-Y. Kim, "Skeleton-based dynamic hand gesture recognition using a part-based gru-rnn for gesture-based interface," *Ieee Access* **8**, 50236–50243 (2020).

41. K. Lai and S. N. Yanushkevich, "Cnn+ rnn depth and skeleton based dynamic hand gesture recognition," in *2018 24th international conference on pattern recognition (ICPR)*, (IEEE, 2018), pp. 3451–3456.

42. A. D'Eusonio, A. Simoni, S. Pini, *et al.*, "A transformer-based network for dynamic hand gesture recognition," in *2020 International Conference on 3D Vision (3DV)*, (IEEE, 2020), pp. 623–632.

43. G. C. Silvestre, F. Balado, O. Akinremi, and M. Ramo, "Online gesture recognition using transformer and natural language processing," *arXiv preprint arXiv:2305.03407* (2023).

44. S. Hampali, S. D. Sarkar, M. Rad, and V. Lepetit, "Keypoint transformer: Solving joint identification in challenging hands and object interactions for accurate 3d pose estimation," in *Proceedings of the IEEE/CVF Conference on Computer Vision and Pattern Recognition*, (2022), pp. 11090–11100.

45. T. Ohkawa, K. He, F. Sener, *et al.*, "Assemblyhands: Towards egocentric activity understanding via 3d hand pose estimation," in *Proceedings of the IEEE/CVF conference on computer vision and pattern recognition*, (2023), pp. 12999–13008.

46. J. Park, G. Moon, W. Xu, *et al.*, "3d hand sequence recovery from real blurry images and event stream," in *European Conference on Computer Vision*, (Springer, 2024), pp. 343–359.

47. S. Zou, C. Guo, X. Zuo, *et al.*, "Eventhpe: Event-based 3d human pose and shape estimation," in *Proceedings of the IEEE/CVF International Conference on Computer Vision*, (2021), pp. 10996–11005.

48. E. Calabrese, G. Taverni, C. Awai Easthope, *et al.*, "Dhp19: Dynamic vision sensor 3d human pose dataset," in *Proceedings of the IEEE/CVF conference on computer vision and pattern recognition workshops*, (2019), pp. 0–0.

49. J. Chen, H. Shi, Y. Ye, *et al.*, "Efficient human pose estimation via 3d event point cloud," in *2022 International Conference on 3D Vision (3DV)*, (IEEE, 2022), pp. 1–10.

50. J.-M. Maro, S.-H. Ieng, and R. Benosman, "Event-based gesture recognition with dynamic background suppression using smartphone computational capabilities," *Front. neuroscience* **14**, 275 (2020).

51. R. Tapiador-Morales, J.-M. Maro, A. Jimenez-Fernandez, *et al.*, "Event-based gesture recognition through a hierarchy of time-surfaces for fpga," *Sensors* **20**, 3404 (2020).

52. Q. Chen, Z. Wang, S.-C. Liu, and C. Gao, "3et: Efficient event-based eye tracking using a change-based convlstm network," in *2023 IEEE Biomedical Circuits and Systems Conference (BioCAS)*, (IEEE, 2023), pp. 1–5.

53. N. Li, M. Chang, and A. Raychowdhury, "E-gaze: Gaze estimation with event camera," *IEEE Trans. on Pattern Anal. Mach. Intell.* **46**, 4796–4811 (2024).

54. T. Stoffregen, H. Daraei, C. Robinson, and A. Fix, "Event-based kilohertz eye tracking using coded differential lighting," in *Proceedings of the IEEE/CVF Winter Conference on Applications of Computer Vision*, (2022), pp. 2515–2523.

55. A. N. Angelopoulos, J. N. Martel, A. P. Kohli, *et al.*, "Event based, near eye gaze tracking beyond 10,000 hz," *arXiv preprint arXiv:2004.03577* (2020).

56. A. Vasudevan, P. Negri, C. Di Ielsi, *et al.*, "Sl-animals-dvs: event-driven sign language animals dataset," *Pattern Anal. Appl.* pp. 1–16 (2022).

57. P. Zhang, H. Yin, Z. Wang, *et al.*, "Evsign: Sign language recognition and translation with streaming events," in *European Conference on Computer Vision*, (Springer, 2024), pp. 335–351.

58. J. Yuan, H. Li, Y. Peng, *et al.*, "Event-based head pose estimation: Benchmark and method," in *European Conference on Computer Vision*, (Springer, 2024), pp. 191–208.

59. P. Bhattacharyya, J. Mitton, R. Page, *et al.*, "Helios: An extremely low power event-based gesture recognition for always-on smart eyewear," *arXiv preprint arXiv:2407.05206* (2024).

60. J. Jiang, J. Li, B. Zhang, *et al.*, "Evhandpose: Event-based 3d hand pose estimation with sparse supervision," *IEEE Trans. on Pattern Anal. Mach. Intell.* (2024).

61. C. Millerdurai, D. Luvizon, V. Rudnev, *et al.*, "3d pose estimation of two interacting hands from a monocular event camera," in *2024 International Conference on 3D Vision (3DV)*, (IEEE, 2024), pp. 291–301.

62. W. Chen, S.-C. Liu, and J. Zhang, "Ehoa: A benchmark for task-oriented hand-object action recognition via event vision," *IEEE Trans. on Ind. Informatics* (2024).

63. J. Jiang, X. Zhou, B. Wang, *et al.*, "Complementing event streams and rgb frames for hand mesh reconstruction," in *Proceedings of the IEEE/CVF Conference on Computer Vision and Pattern Recognition*, (2024), pp. 24944–24954.

64. C. Plizzari, M. Planamente, G. Goletto, *et al.*, “E2 (go) motion: Motion augmented event stream for egocentric action recognition,” in *Proceedings of the IEEE/CVF conference on computer vision and pattern recognition*, (2022), pp. 19935–19947.
65. M. P. E. Apolinario and K. Roy, “S-tllr: Stdip-inspired temporal local learning rule for spiking neural networks,” arXiv preprint arXiv:2306.15220 (2023).